AD-A219 509

REPORT DOCUMENTATION PAGE

Form Approved
OMB No. 0704-0188

1. AGENCY USE ONLY (Leave blank)	2. REPORT DATE February 28, 1990	3. REPORT TYPE AND DATES COVERED Final, Aug. 10, 1988 – Feb. 28, 1990

4. TITLE AND SUBTITLE	5. FUNDING NUMBERS
Evaluation of Space Plasma Data: Effects Upon Spacecraft Materials and Predictions of Hazardous Conditions; Polar Arcs. Final Report	DLA 900-84-C-0910 CLIN 0001 AE

6. AUTHOR(S)

L.A. Weiss, J.D. Winningham, J.R. Sharber

7. PERFORMING ORGANIZATION NAME(S) AND ADDRESS(ES) Southwest Research Institute 6220 Culebra Road San Antonio TX 78238	8. PERFORMING ORGANIZATION REPORT NUMBER 17-7958-801-01

9. SPONSORING/MONITORING AGENCY NAME(S) AND ADDRESS(ES) Sponsor: Air Force Geophysics Laboratory/XOR Hanscom AFB MA 01731-5000 Monitor: Defense Electronics Supply Center Dayton, Ohio 45444-5208	10. SPONSORING/MONITORING AGENCY REPORT NUMBER

11. SUPPLEMENTARY NOTES

DTIC
ELECTE
MAR 2 1 1990
S D

12a. DISTRIBUTION/AVAILABILITY STATEMENT Unlimited	12b. DISTRIBUTION CODE

13. ABSTRACT (Maximum 200 words)

The Polar ARCS campaign consisted of a highly coordinated set of ground based, airborne, and in situ measurements of a polar cap aurora over Sondrestrom, Greenland, on February 26, 1987. Three charges of barium were injected into the F-region ionosphere immediately prior to the launch of a Black Brant IX rocket instrumented with AC and DC magnetometers, plasma wave and electric field probes, and ion/neurtal and electron spectrometers. Simultaneous electron density and line-of-sight measurements were made by the Sondrestrom incoherent scatter radar, and all-sky imaging photography was performed by the AFGL Airborne Ionospheric Observatory (AIO).

This report discusses the electron measurements and data analysis, performed by Southwest Research Institute under Contract No. DLA 900-84-C-0910 CLIN 0001AE. Interplanetary magnetic field (IMF) and DMSP satellite data are presented in an attempt to establish the global morphology of the polar cap during the campaign. The current status of the data from each of the other instruments is also assessed and recommendations for further data analysis are made.

14. SUBJECT TERMS Polar cap aurora; ionospheric disturbances; ionospheric irregularities			15. NUMBER OF PAGES 35
			16. PRICE CODE

17. SECURITY CLASSIFICATION OF REPORT Unclassified	18. SECURITY CLASSIFICATION OF THIS PAGE Unclassified	19. SECURITY CLASSIFICATION OF ABSTRACT Unclassified	20. LIMITATION OF ABSTRACT SAR

1. Introduction

The Polar ARCS campaign consisted of a highly coordinated set of ground based, airborne, and in situ measurements of a polar cap aurora over Sondrestrom, Greenland, on February 26, 1987. Three charges of barium ions were injected into the F-region ionosphere immediately prior to the launch of a Black Brant IX rocket instrumented with AC and DC magnetometers, plasma wave and electric field probes, and ion/neutral and electron spectrometers. Simultaneous electron density and line-of-sight velocity measurements were made by the Sondrestrom Incoherent Scatter Radar, and all-sky imaging photography was performed from the AFGL Airborne Ionospheric Observatory (AIO).

The instrumented rocket was launched at 2349:10 UT to the northeast, reaching an apogee of 380 km and covering a ground range of 166 km. Launch criteria included verification by the AIO of stable, sun-aligned arcs within the predicted payload trajectory, clear skys at both Sondrestrom and Thule, and a sunlit F-region over dark skies for successful optical imaging of the barium clouds. At T0 + 65 seconds, the nosecone (daughter) portion of the rocket separated from the main payload in order to provide a magnetically clean environment for the DC science magnetometer aboard. Both 'mother' and 'daughter' followed essentially the same trajectory thereafter, separated by a distance of 1.34 km at apogee. Data was obtained from both payloads for nearly 600 seconds after launch.

Figure 1 displays a series of 6300 Å [OI] images at 30-second intervals obtained prior to and during the rocket flight using a wide angle (155° field-of-view) all-sky imaging photometer (ASIP) [*Weber et al..*, 1977]. The field-of-view for these images is about 1200 km, assuming an emission height of 250 km. In the images, the stars at

90 33 20 029

2347:30, 2350:00, and 2352:00 UT represent the three barium releases and the black dots indicate the position of the rocket (both mapped to an altitude of 250 km).

Shortly after the decision to launch was made, the polar cap arcs observed by ASIP began to fade in brightness. As can be seen in Figure 1, the arcs started fading at about 2350 UT, from a pre-launch brightness of about 300 R to less than 100 R at 2353 UT [*E.J. Weber*, private communication, 1990]. The diminished optical emissions are certainly indicative of a reduction in the flux of low energy (< 1 keV) electrons reaching the altitudes associated with 6300Å emissions (200 - 300 km). Correspondingly low values of F-region electron densities and field-aligned currents were measured, making a detailed analysis of the electrodynamic circuitry of the arc difficult. Although the fading of the arc was unfortunate, some valuable information can still be gained from the measurements.

Section 2 of this report will concentrate on the electron measurements and data analysis performed by Southwest Research Institute under Contract No. DLA 900-84-C-0910 CLIN 0001AE. IMF and DMSP data are presented in Sections 3 and 4, respectively, in an attempt to establish the global morphology of the polar cap during the campaign. In the last section, the current status of the data from each of the other instruments is assessed and recommendations for further data analysis are made.

2. Electron Spectrometer Measurements

The electron measurements in the 1.0 eV - 13.3 keV energy range were made using a 'tophat' electrostatic analyzer [*Sharber et al.*,1988]. The deflection plate voltage was stepped in 64 logrithmically spaced increments. A complete spectral measurement was made every 256 ms. Incoming electrons from a 360° planar field-of-view were detected at the exit plane by eleven equally spaced channeltrons. Because the instrument was mounted with its acceptance plane parallel to the rocket's spin axis, each of the eleven
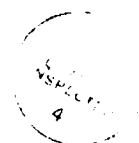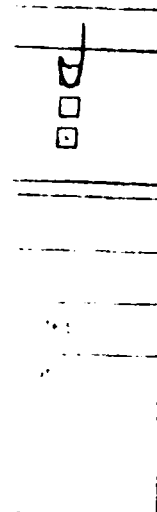
A-1

sensors sampled a different range of pitch angles during a single spin of the rocket. The pitch angle range of each sensor changed continuously throughout the flight since the rocket's spin axis was maintained along its ram direction. The spectral measurements display a relatively low signal-to-noise ratio due to a strong noise source coupled with the unexpectedly low count rates encountered in the fading, sub-visual arc. Steps have been taken to obtain an estimate of the true count rate signal by removing the noise. Details on the pitch angle calculations and the noise reduction scheme are described in Appendices A and B, respectively.

The electron precipation measured by two conjugate sensors on the tophat analyzer is shown in Figure 2. The top spectrogram shows data from sensor 6, which sampled downcoming electrons on the upleg of the flight; the lower spectrogram displays data from sensor 9, which measured upcoming electrons on the upleg. The pitch angles sampled by these sensors are shown in Figure 3.

Three electron precipation events were detected during the flight and can be identified on the spectrogram in the intervals 2351:54 - 2352:30 UT, 2353:27 - 2354:25 UT, and 2356:38 - 2357:22 UT. The events have the appearance of high latitude arcs but are very narrow in extent, the widest being only on the order of 10 km. Since the rocket's total ground range was only 167 km, (compared to an image diameter of nearly 1200 km) it is clear that the structures seen by the electron spectrometer were spatial or temporal enhancements of a scale size not resolvable in the images in Figure 1.

The precipating energy flux profiles (ergs / cm^2 sec) in the energy range 1.0 ev - 1.0 keV integrated over the downcoming hemisphere for the first two precipitation events are shown in Figure 4. In calculating these fluxes, the noise and the relatively low count rates made it necessary to average the spectral data over several seconds. Because the noise level varied from sensor to sensor, it was also felt best to restrict the analysis to individual sensors. The histograms of Figure 4 were computed using five second

averages of the counts from sensor 6. The precipitating electrons were assumed to be isotropic over the downcoming hemisphere. This type of calculation can be used to estimate the 6300 Å emission based on the method by *Shepherd et al.* [1980]. The total downcoming energy fluxes in the energy bands 5 - 60 eV, 60 - 300 eV, and 0.3 - 1 keV have been computed and multiplied by empirically determined 6300 Å production coefficients, yielding emissions of 85 R and 44 R at the peaks of the first and second events, respectively.

The ambient ionospheric conductivity during the rocket flight has been calculated using three different types of data. In all three cases, an altitude profile of electron number density was combined with a model of collision frequencies to compute the height profiles of Pedersen and Hall conductivity. The resulting conductivity profiles are shown in Figure 5. In the first method and second methods, the electron number density profiles were measured by the Pulsed Plasma Probe (Langmuir probe) and radar, respectively. The third method used the 5-second average electron number flux spectra at the peak of the first event as input to the energy deposition code TANGLE [*Vondrak and Baron*, 1976; *Vickrey*, et al., 1981, *R.M. Robinson*, private communication, 1990] to produce the required electron number density profile.

As can be seen in Figure 5, the radar and Langmuir probe profiles are similar, yielding values for the height-integrated Pedersen conductivity of 0.58 mho and 1.68 mho, respectively. The TANGLE profile, on the other hand, corresponds to a height-integrated Pedersen conductivity of only 0.1 mho. Since the TANGLE calculation cuts off at an altitude of 200 km, it is evident that either significant ionization is occurring above 200 km or a significant amount of solar-produced ionization is convecting into the region from sunlit areas. The weak nature of the precipitation events and lack of structure in the radar electron number density and temperature contour plots favor the latter explanation.

A calculation of the height-integrated Pedersen and Hall conductivities as a function of rocket range will be made using the electron number flux spectra and the Strickland electron flux transport code [Strickland, 1976] in conjunction with an ionospheric chemistry model to determine the electron density profiles. Once the electric field measurements are obtained from NRL, it will be possible to combine E with the derived values of $\Sigma_p(x)$ and $\Sigma_h(x)$ to obtain $J_\perp$ and $J_{||}$, the horizontal and field-aligned currents flowing in the vicinity of the three events.

3. Geomagnetic and IMF conditions

During the Polar ARCS campaign the IMP 8 spacecraft was located in the downstream solar wind (SM coordinates: $-26R_E$ x, $27R_E$ y, $-1.2R_E$ z). The vector components and total field stength of the IMF for the 2 hours before and 1 hour after launch are shown in Figure 6. Assuming an average solar wind speed of 400 km/sec, IMF conditions over the polar cap at the time of the launch would be measured by the spacecraft approximately 7 minutes later. This time is indicated by the dashed line on the plot. The geomagnetic three-hourly average K_p indices for the intervals 2100 - 0000 UT and 0000 - 0300 UT were both 1, indicating nominal magnetospheric activity.

For nearly five hours prior to the launch of the rocket, B_z was strongly positive (on the order of +5 nT), but turned southward at 2315 UT. B_z remained southward for approximately 45 minutes, turning weakly northward by the time of launch. B_x is predominently negative during the time span of negative B_z, as would be expected for a downstream satellite below the equatorial plane. B_y is chaotic and shows no predominant trends.

4. Global Morphology

Simultaneous optical and electron flux measurements from two DMSP satellite

northern hemisphere passes at the time of the rocket flight have been analyzed in conjunction with the IMF data in order to establish the global morphology of the polar cap during the experiment. Figure 7 is an MLT / IL plot of the ground trajectories of the DMSP satellites and the track of the Soundrestom ground station. Each trajectory is labeled with time markers in UT. The position of the auroral oval, inferred from the DMSP electron measurements, has also been noted. In this coordinate system, the long axes of the arcs in Figure 1 are oriented slightly west (~30°) of magnetic north. This orientation aligns them with the evening side of the auroral oval in Figure 7.

Number flux spectrograms from the (dawn-dusk) F6 overpass and the (noon-midnight) F7 overpass are shown in Figure 8. Enhanced electron and ion precipitation over the middle of the polar cap at 0012 UT in Figure 8 (a) indicates the presence of a transpolar aurora at the time of the pass. It is possible that the polar cap is in a very contracted state and that the arc at 0012 UT represents the poleward edge of an expanded duskside auroral oval, a configuration which has also been proposed for certain northward B_z conditions by *Murphree* [*et al.*, 1982, 1989] and *Meng* [1981].

5. Status of Supplementary Data Sets

5.1. Radar Measurements

Prior to and during the rocket flight, the Sondrestrom incoherent scatter radar operated in a mode combining both azimuth and elevation scans of the region traversed by the rocket. The normal mode allowed for one 20° - 60° elevation scan at 51° azimuth (magnetic E-W), followed by a set of 3 partial azimuth scans at a fixed elevation of 35°. The first azimuth scan was from 51° to -39°, followed by a scan from -39° to 141°, and ending with a scan from 141° to 51°. From 2342:06 to 2359:45 UT repeated elevation scans with one second integration were performed. At 2359:45 UT the normal sequence of 3 azimuth scans followed by an elevation scan was resumed, with 5 second integration

time.

Figure 9 shows electron density contours and line-of-sight velocity measurements for three scans made during the flight. The first two panals are partial azimuth scans made prior to the rocket launch. Some regions of enhanced number density can be seen to the east in (a) and to the north in (b). Panel (c) is an elevation scan completed just as the rocket was launched. The rocket trajectory is noted on the plot. In an effort to adequately sample the E-region parameters, the 20° - 60° elevation scans made during the rocket flight sampled regions significantly below and to the northeast of the region traversed by the rocket. For this reason, it is not possible to use the radar measurements to compute the electric fields and Pedersen conductivity in the three events noted on the spectrograms. The radar measured number densities were used to calculate the ambient ionospheric conductivity, however. The number density profile at a range of 250 km in the elevation scan in (c) was used in conjunction with a model of collision frequencies to compute the height profile of Pedersen conductivity seen in Figure 5. A more detailed description of this calculation can be found in Section 5.4.

5.2. Magnetic Field Measurements

A three-axis fluxgate magnetometer designed to measure magnetic fields in the range ±60,000 nT [*Primdahl*, 1979] was mounted on the daughter module for the purpose of measuring magnetic field perturbations due to the presence of field-aligned currents in the region traversed by the rocket. Three components of the magnetic field were sampled at a rate of 125 sec^{-1}. Subsequent data analysis involved subtracting the components from those of an IGRF model to obtain the residual field components, then rotating the residuals into a magnetic coordinate system with the z axis antiparallel to the earth's main field and the x axis pointing northward in the magnetic meridian plane [*Primdahl and Marklund*, 1986]. This coordinate system is particularly well suited for the display of the

magnetic perturbations from Birkeland currents since a large gradient in the perturbation field is expected in the component parallel to a sheet current when it is crossed.

Figures 10 (a) and (b) are plots of the magnetic north-south and east-west components of the perturbation field. The sharp positive and negative gradients are identified as regions of upward and downward field-aligned currents. From the scale used in plotting Figure 10 it is clear that very little current was being drawn from the ionosphere in the vicinity of the three precipitation events. The largest perturbation was seen near the dusk side of the first event (T0+180 - T0+190 seconds) in Figure 10 (b), where a 7.25 nT deviation was recorded. If the precipitation events are aligned with the larger arc systems seen in Figure 1, this deviation occurs in the component most nearly perpendicular to the long axis of the arc, indicating either a downward filamentary current or a sheet-like current crossing the arc. Neither of these orientations of the current structure agree with the popular model that arcs are associated with upward field-aligned currents distributed along the long axis of the arc.

Given the extremely small size and unusual orientation of the auroral current, it is felt that further analysis of the electrodynamic structure of the arcs cannot proceed until comparison with the electric field data can be made. *Sugiura* [*et al..*, 1982; 1984] has demonstrated an extremely high correlation between the component of the perturbation field parallel to a field-aligned current sheet (δB_y) and the cross-sheet component of the electric field (E_x). This correlation will be used to verify the orientation of the magnetometer-derived current, and the values of E, when combined with the conductivities, will give an independent measure of the current structure near the arcs.

5.3. Barium Release

Six minutes prior to the launch of the instrumented payload, a Taurus - Nike - Tomahawk rocket carrying three shaped charges of neutral barium / strontium was

launched into the sunlit F-region ionosphere. The first release occurred at 110 seconds before launch (2347:20 UT), followed by a second release at T0+ 50 sec (2350 UT) and a third at T0+150 sec (2351:40 UT). Observing sites at Sondrestom, Dye 2, and Jakobshavn photographically recorded the horizontal convection and field-aligned acceleration of the ionized barium clouds. The direction angles of the lines-of-sight from the photographs from two or three of the sites were used to locate the position of the release points and of the subsequent lines of ionized barium forming along the earth's magnetic field lines. The relative position of the three barium jets, the rocket's ground trajectory, and the three precipation events are plotted in Figure 11. The three observation sights and the rocket range east of Sondrestrom have also been noted.

The time markers along each of the barium trajectories in Figure 11 are in minutes after 2300 UT. The neutral barium / strontium clouds are indicated by points, and the bottom of the ionized barium striations (projected to a surface of 100 km) are indicated by transverse bars. Striations of a single jet are connected by dashed lines. When the same cloud or line is triangulated by two or three pairs of stations the positions are circled. The neutral clouds can be seen to move generally in the direction of the rocket trajectory, whereas the ionized jets are drifting to the southwest, along the magnetic meridian.

The coordinates of the projected, lowest points of the barium jets normal to and parallel to the local magnetic meridian plane are plotted versus time in Figures 12 and 13, respectively [courtesy of *I.S. Mikkelsen*, Division of Geophysics, DMI]. Figure 12 shows a small eastward velocity of approximately 88 m/s. The equivalent northward electric field is -4.7 mV/m. Figure 13 shows a southward motion that speeds up from a velocity of -134 m/s prior to 23:50 UT to -420 m/s, corresponding to eastward electric fields of -7.0 mV/m and -21.9 mV/m respectively [*Mikkelsen*, 1987]. These values will be compared to the electric field probe data when it becomes available.

Observations of the upper and lower tips of the barium jets as they accelerate along

the magnetic field lines provide the best direct estimate of the parallel electric field structure above the arcs. This analysis has been performed by Gene Wescott of the University of Alaska.

5.4. Langmuir Probe (Pulsed Plasma Probe)

The height profile of electron number density from the upleg of the rocket flight has been used to compute both the ion-neutral collision frequency (v_{in}) and Pedersen conductivity (σ_p) as a function of altitude. The model used for the collision frequency is:

$$v_{in} = 2.6 \times 10^{-9} (N_n + N_i) A^{-1/2}$$

where N_n and N_i are the number densities of the neutrals and ions, respectively, in cm^{-3}. The collision frequency profile, shown in Figure 14, was computed using the measured electron number densities at 20 km increments from 120-380 km and MSIS 83 model values for N_n. The altitude profiles of Pedersen conductivity, shown previously in Figure 5 were calculated using the relation:

$$\sigma_p = \frac{eN_e}{B} \left[\frac{v_{in} \omega_i}{\omega_i^2 + v_{in}^2} \right]$$

where e is the charge of the electron, N_e is the electron number density in m^{-3}, B is the magnetic field strength in tesla, and ω_i is the ion gyrofrequency. Since the ratio of the electron gyro to collision frequency becomes very large above 75 km, a second term involving v_{en} and ω_e has been neglected.

5.5. Ion / Neutral Mass Spectrometer

The data from the Ion / Neutral Mass Spectrometer has been reduced and analyzed by John Ballenthin of AFGL. Height profiles of ions and neutrals have been calculated and are available for use.

5.6. *Electric Field*

As of the time of this report, the Electric Field Probe data to be supplied by NRL has not been reduced.

Appendix A: Pitch Angle Calculations

In order to compute the pitch angle of each of the tophat sensors, a knowledge of the vector magnetic field at the instrument is required. Normally, the components of the earth's magnetic field along three mutually perpendicular rocket axes are measured by an on-board aspect magnetometer. The unit vectors b_x, b_y and b_z are then dotted with the normal unit vector of each sensor, ϑ_i, to yield the pitch angles, α_i:

$$\cos\alpha_i = b_x\cos\vartheta_i + b_y\cos45°\sin\vartheta_i + b_z\sin45°\sin\vartheta_i \ .$$

The cos45° and sin45° terms indicate that in this case the tophat's axis of rotation was oriented at 45° between the rocket y and z axes (the x axis was defined as being along the spin axis of the rocket).

Unfortunately, the presence of an extraneous magnetic field on the 'mother' rocket corrupted the aspect magnetic field measurements. Since the measurements could not be used, a magnetic field model (MAGSAT) was used to obtain the field along the rocket's trajectory. The geocentric spherical components (B_r, B_φ, and B_ϕ) returned by the model were converted into the rocket's coordinate system by using transformation equations involving the Euler pitch, yaw and roll angles provided by the on-board gyros. The pitch angles were then computed as described above.

Appendix B: Noise Reduction

During the flight the electron spectrometer sensors displayed noise levels observed to be proportional to their count rates. The noise is not uniform in every channel or even over the time of flight in one channel, but rather rises and falls in proportion to the measured signal. The noise is believed to be caused by electromagnetic interference (EMI) from electronics associated with the tophat analyzer or other nearby instruments. This is consistent with the observation that as the rocket enters regions of enhanced precipitation the noise increases.

In order to reconstruct the true count rate spectra, a unique level of background noise was subtracted from each sweep of raw data. The number of counts subtracted was determined by smoothing each spectrum and then averaging the smoothed counts from the 15 highest energy steps (corresponding to energies between 1.4 and 13.2 keV) to obtain the average background count for that sweep. Since the arcs measured on this flight were sub-visual, low-energy polar cap arcs, we are confident in assuming that most of the counts in these energy bins were noise-induced.

References

Meng, C.-I., Polar cap arcs and the plasma sheet, *Geophys. Res. Lett.*, 8, 273, 1981.

Mikkelsen, I.S., Drift of the Ba-jets released over Greenland on February 26 and March5, 1987, *Progress Report* for grant AFOSR-87-0203, Division of Geophysics, Danish Meteorological Institute, Copenhagen, Denmark, 1987.

Murphree, J.S., C.D. Anger, and L.L. Cogger, The instantaneous relationship between polar cap and oval auroras at times of northward interplanetary magnetic field, *Can. J. Phys.*, 60, 349, 1982.

Murphree, J.S., R.D. Elphinstone, L.L. Cogger, and D.D. Wallis, Short-term dynamics of the high-latitude auroral distribution, *J. Geophys. Res.*, 94, 6969, 1989.

Primdahl, F., The fluxgate magnetometer, *J. Phys. E: Sci. Instrum..*, 12, 241, 1979.

Primdahl, F., and P.A. Jensen, Compact spherical coil for fluxgate magnetometer vector feedback, *J. Phys. E: Sci. Instrum.*, 15, 221, 1982.

Primdahl, F., and G. Marklund, Birkleland currents correlated with direct-current electric fields observed during the CENTAUR Black Brant X rocket experiment, *Can. J. Phys.*, 64, 1412, 1986.

Sharber, J.R., J.D. Winningham, J.R. Scherrer, M.J. Sablik, C.A. Bargainer, P.A. Jensen, B.J. Mask, N.Eaker, and J.C. Biard, Design, Construction, and Laboratory Calibration of the Angel Resolving Energy Analyzer (AREA): A "Top-Hat" Instrument for Auroral Research, *IEEE Trans. Geosci. Remote Sensing*, 474, 1988.

Shepherd, G.G., J.D. Winningham, F.E. Bunn, and F.W. Thirkettle, An empirical determination of the production efficiency for auroral 6300-Å emission by energetic particles, *J. Geophys. Res.*, 85, 715, 1980.

Strickland, D.J., D.L. Book, T.P. Coffey, and J.A. Fedder, Transport equation techniques for the deposition of auroral electrons, *J. Geophys. Res.*, 81, 2755, 1976.

Sugiura, M., N.C. Maynard, W.H. Farthing, J.P. Heppner, and B.G. Ledley, Initial results on the correlation between the magnetic and electric fields observed from the DE-2 satellite in the field-aligned current regions, *Geophys. Res. Lett.*, 9, 985, 1982.

Sugiura, M., A fundamental magnetosphere-ionosphere coupling mode involving field-aligned currents as deduced from DE-2 observations, *Geophys. Res. Lett.*, 11, 877, 1984.

Weber, E.J., J.Buchau, R.H. Eather, and J.W.F. Lloyd, Large scale optical mapping of the ionosphere, *Rep. AFGL-TR-77-0236,* Air Force Geophys. Lab., Bedford, Mass., 1977.

Figure Captions

Figure 1. All-sky 6300 Å [OI] images of F-layer sun-aligned arcs prior to and during the Polar ARCS rocket flight. The stars represent the three barium releases and the black dots indicate the positon of the rocket.

Figure 2. Energy-time spectrograms of the electron precipitation (counts) in the range 1eV - 13.3 keV as measured by sensors 6 and 9 on the tophat electrostatic analyzer.

Figure 3. Pitch angles sampled by sensors 6 and 9 over the time of flight of the rocket.

Figure 4. Energy flux histograms of downcoming electrons for the first and second precipitation events, computed using five-second averages of the counts from sensor 6.

Figure 5. Pederesen and Hall conductivity profiles computed using (a) radar and (b) langmuir probe electron number density profiles. Profiles (c) were computed using the 5-second average electron number flux spectra at the peak of the first event as input to the TANGLE energy deposition code.

Figure 6. Solar Magnetospheric vector components of the IMF for 2 hours prior to and 1 hour after launch of the Polar ARCS rocket. The dashed line indicates the time at which IMF conditions over the polar cap would be measured by the spacecraft (located in the downstream solar wind) assuming an average solar wind speed of 400 km/s.

Figure 7. An MLT / INVL plot of the ground trajectories of the DMSP satellites and the track of the Sondrestrom ground station. The gray areas indicate the postion of the auroral oval and transpolar arc as *inferred* from the DMSP electron measurements.

Figure 8. (a) Number flux spectrograms of precipitating electrons (top) and ions (bottom) from DMSP F6. (b) Number flux spectrograms of precipitating electrons (top) and ions (bottom) from DMSP F7.

Figure 9. (a) Incoherent scatter radar measurements of electron number density (top) and line-of-sight velocity (bottom) for a 141° - 51° azimuth scan at 2333:07 UT. Regions of enhanced precipitation can be seen directly east of the radar in the top panel. Flows within the region are predominently away from the radar. (b) Similar plots for an azimuth scan from 51° to -39° at 2338:45 UT. (c) Electron number density and LOS velocity measurments from a 20° - 60° elevation scan at 51° azimuth. The rocket trajectory has been noted on the first plot.

Figure 10. (a) Magnetic north-south and (b) magnetic east-west components of the perturbation magnetic field as measured by the science magnetometer.

Figure 11. Relative postions of the the three barium jets (labled in minutes after 2300 UT), the rocket's ground trajectory, and the three precipitation events.

Figure 12. Coordinates of the projected, lowest points of the barium jets normal to the local magnetic meridian plane [from I.S. Mikkelsen, DMI].

Figure 13. Coordinates of the projected, lowest points of the barium jets parallel to the local magnetic meridian plane [from I.S. Mikkelsen, DMI].

Figure 14. Ion - neutral collision frequency profile computed using the Pulsed Plasma Probe electron number density profile and MSIS 83 model values for N_n.
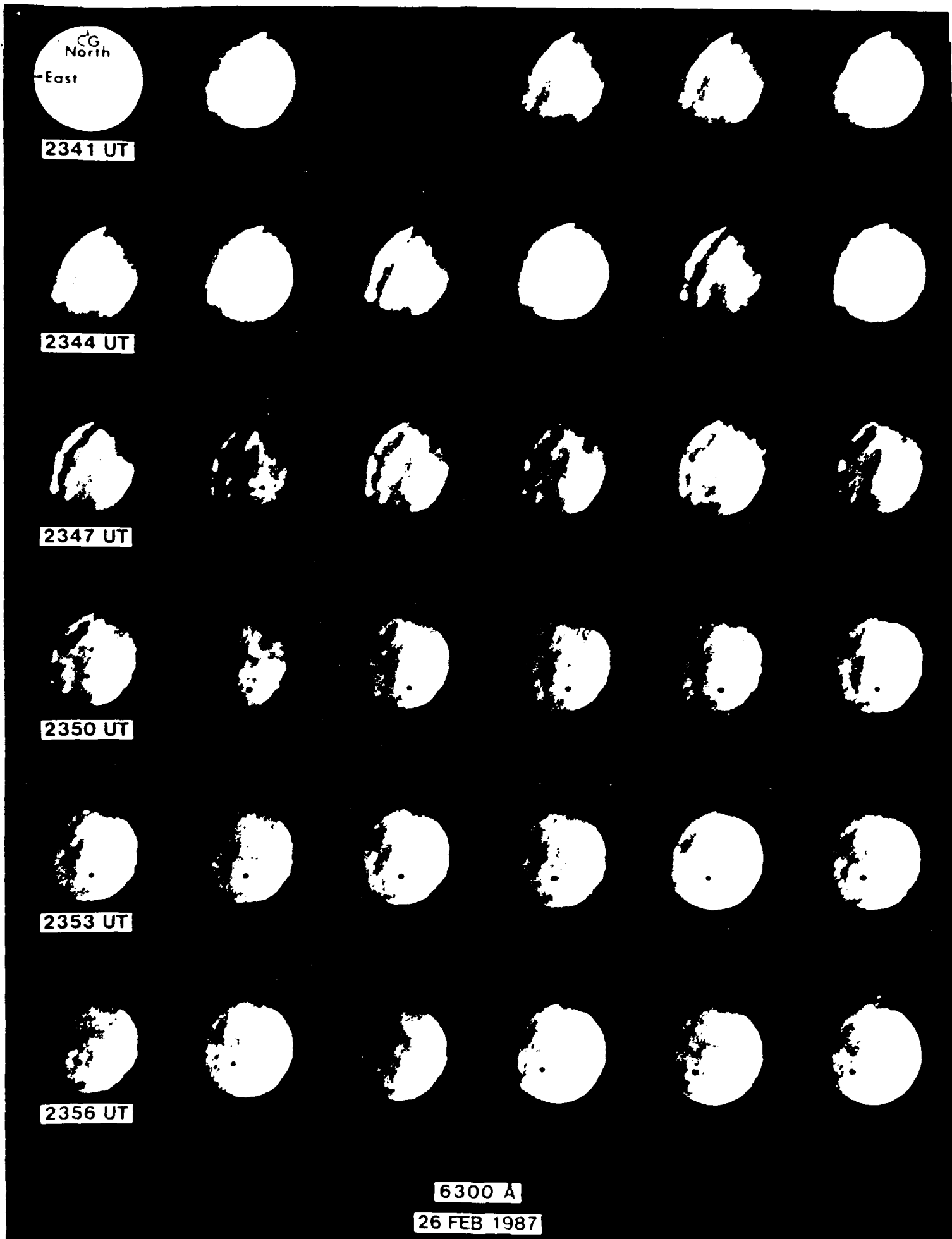
Figure 1
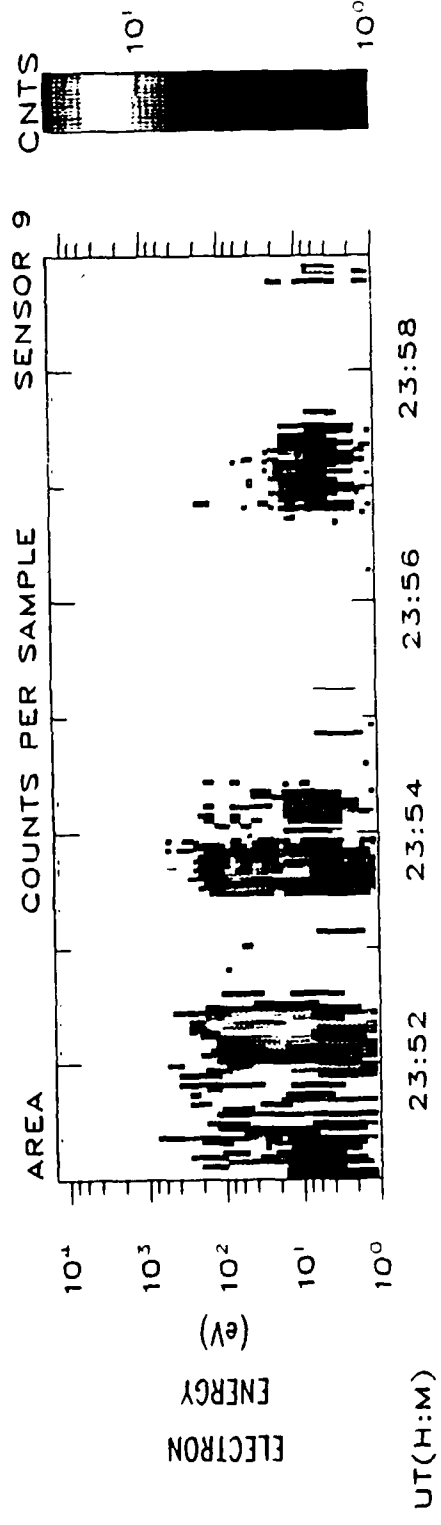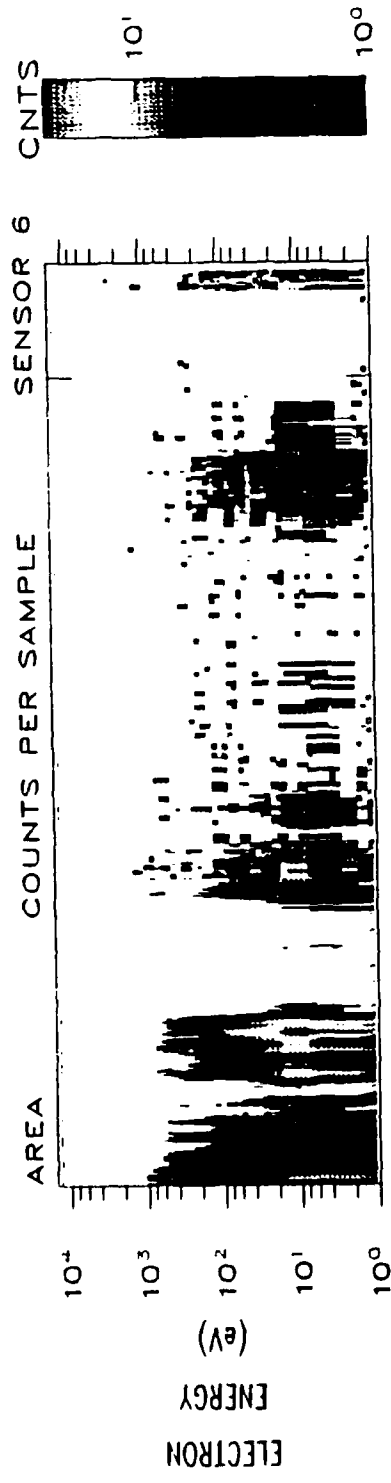
Figure 2

PITCH ANGLE VS. TIME OF FLIGHT

SENSOR 6
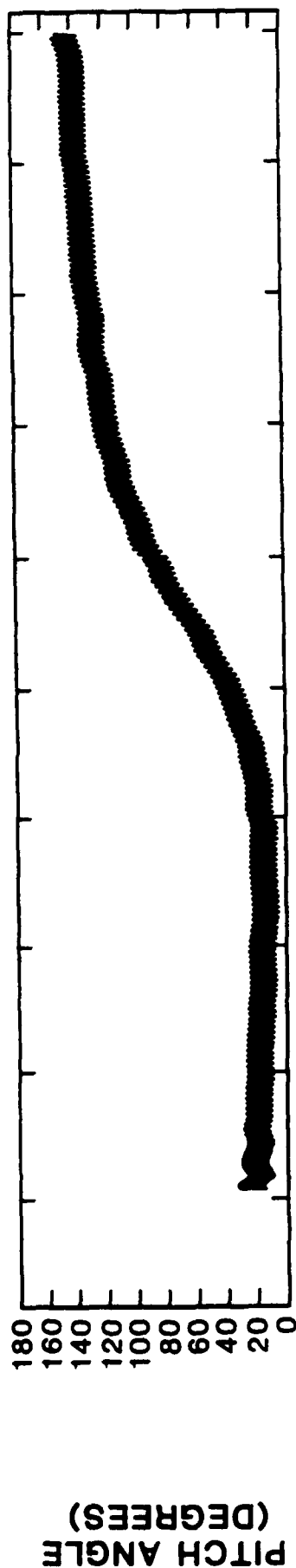
SENSOR 9
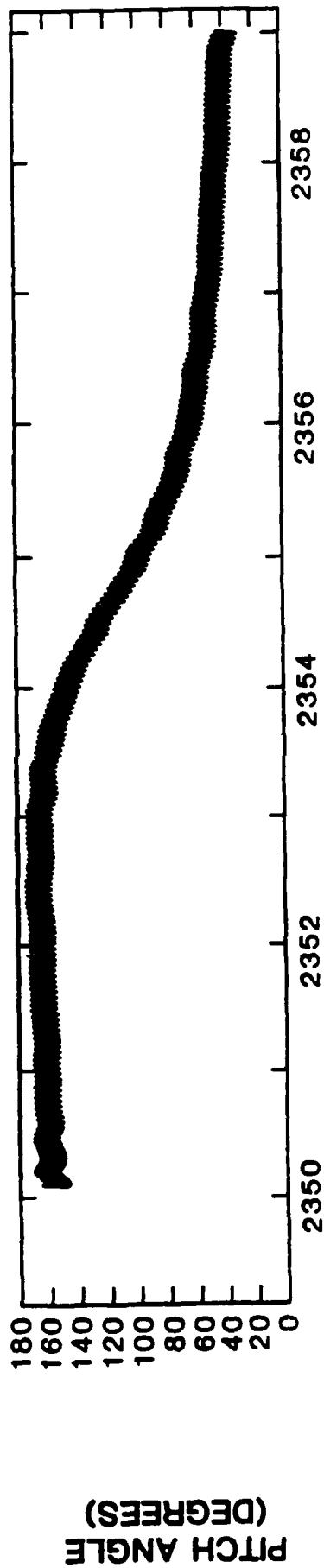
TIME OF FLIGHT (UT)

Figure 3

Figure 4(a)

EVENT 2

UT (min:sec)

ENERGY FLUX (erg/cm²s)
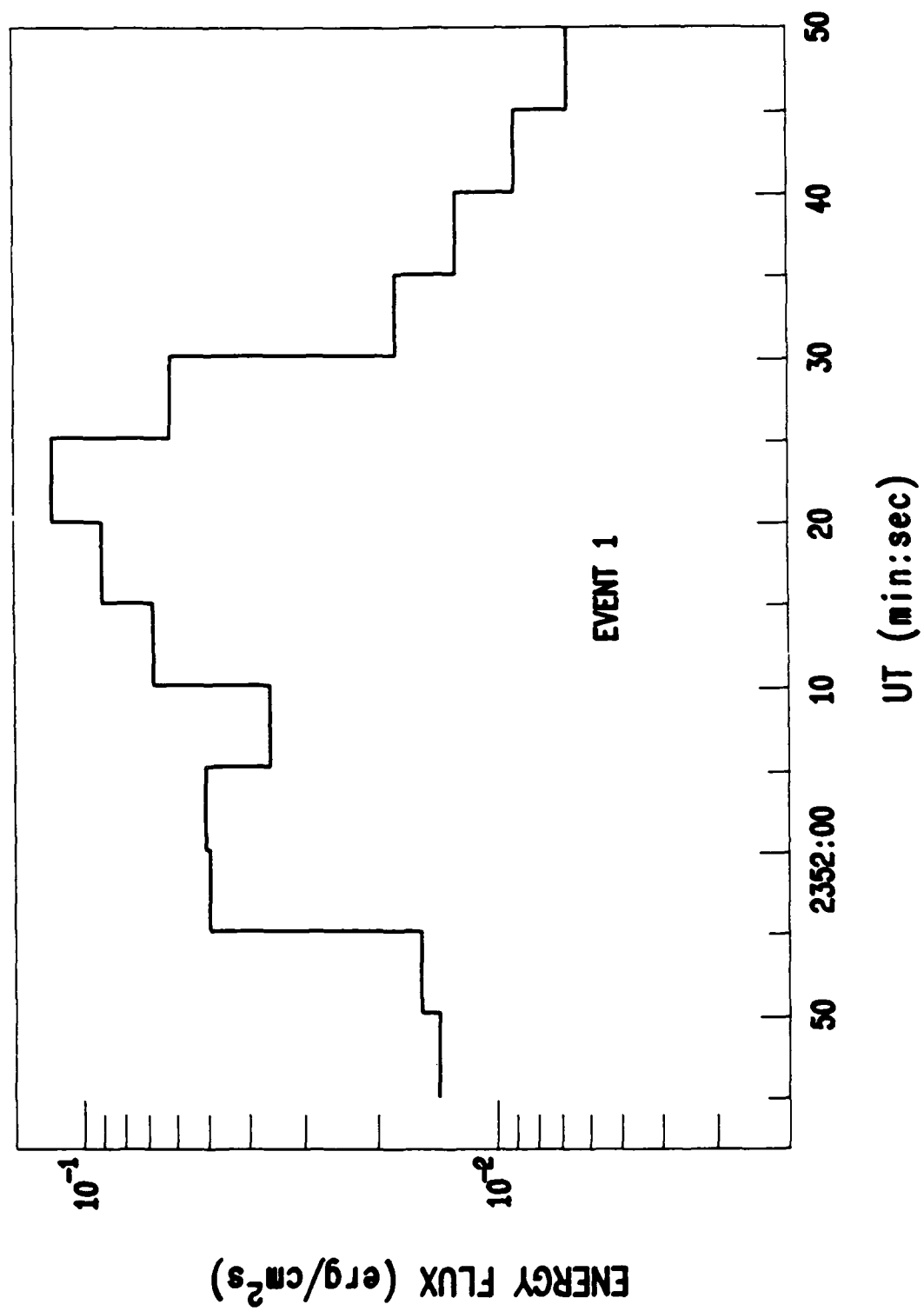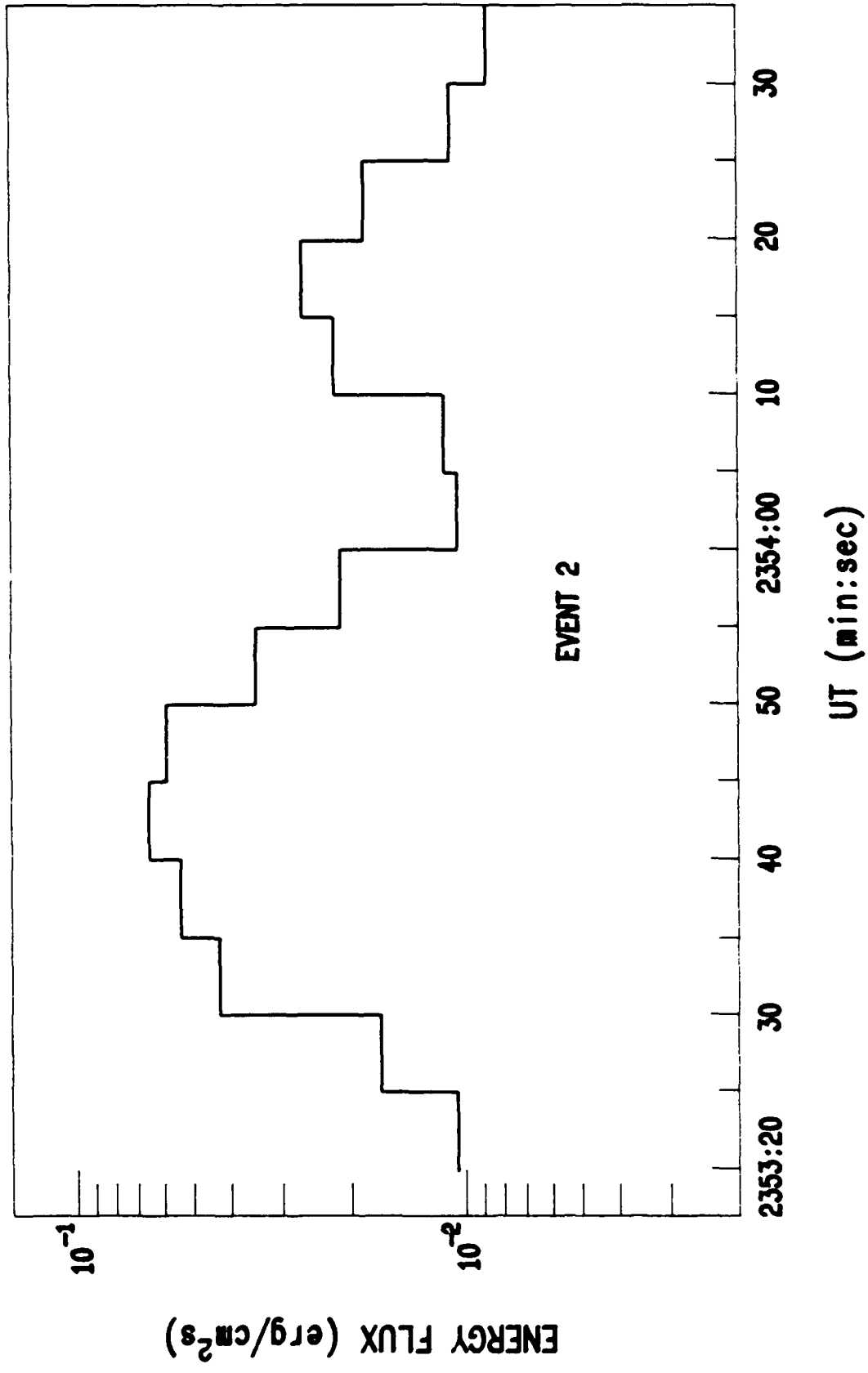
Figure 4 (b)

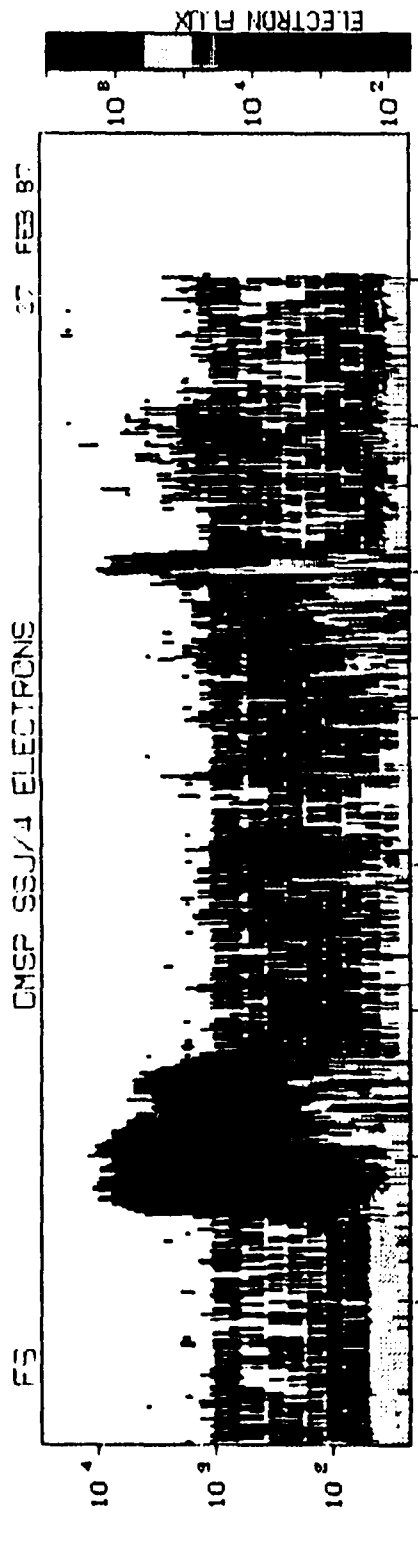PEDERSEN AND HALL CONDUCTIVITY HEIGHT PROFILES
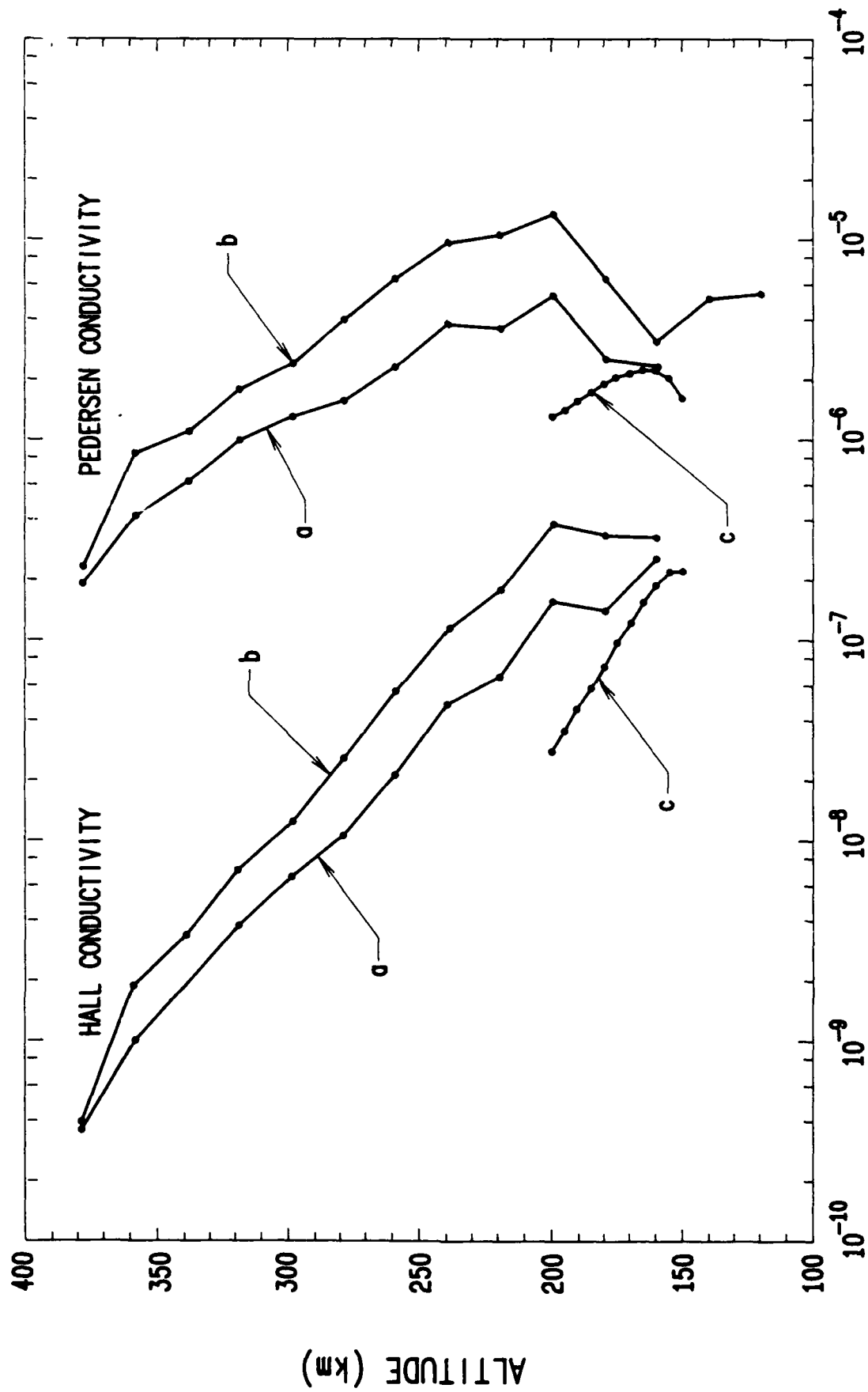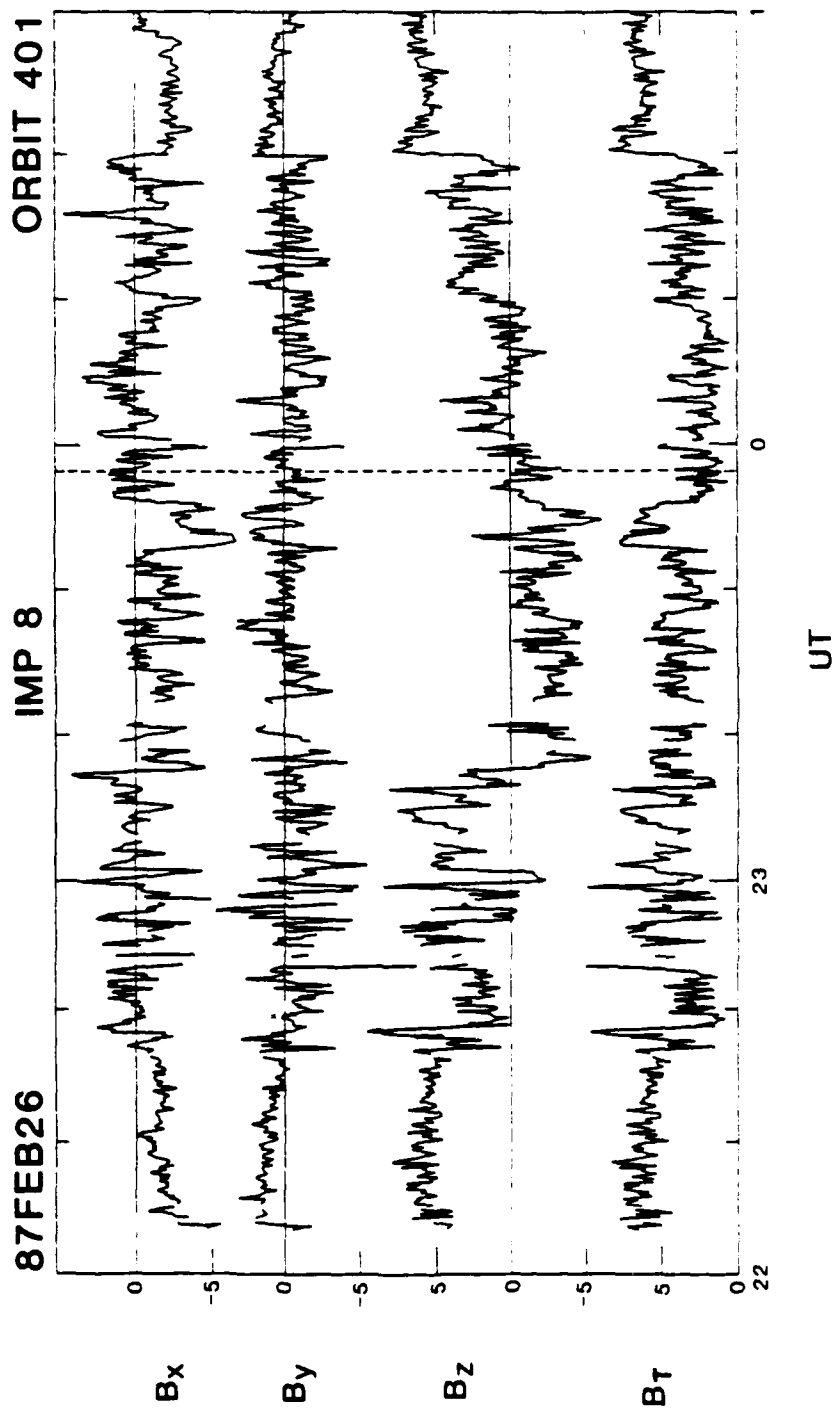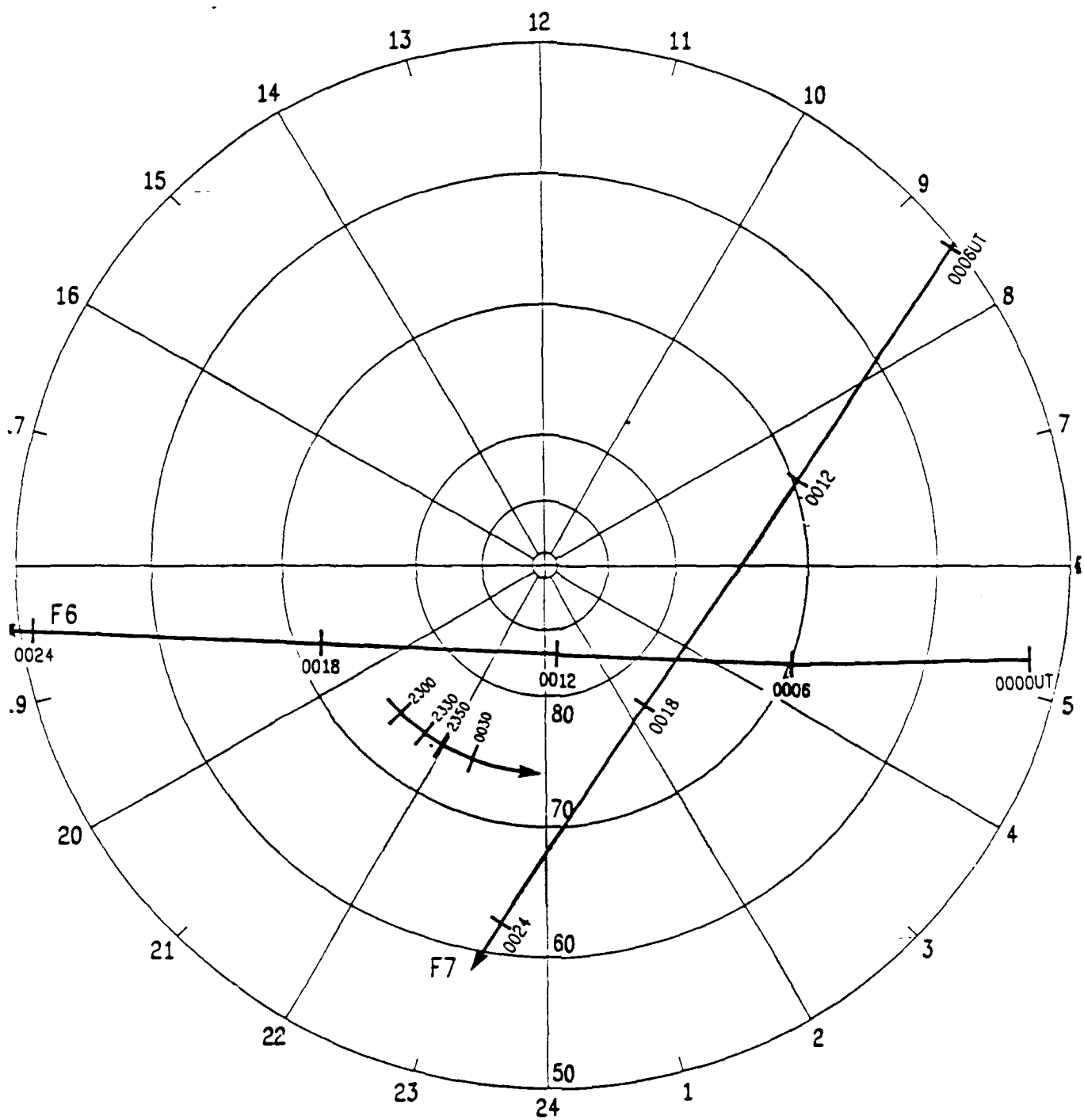
Figure 5

Figure 6

Figure 7

Figure 8 (a)

Figure 8 (b)

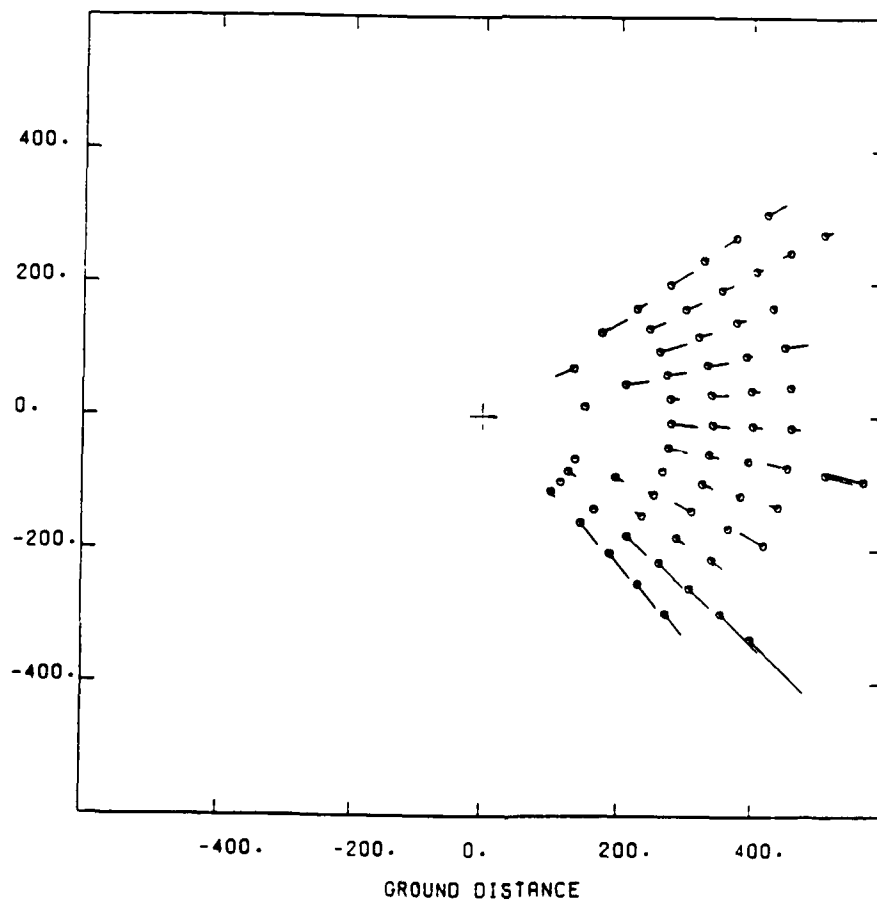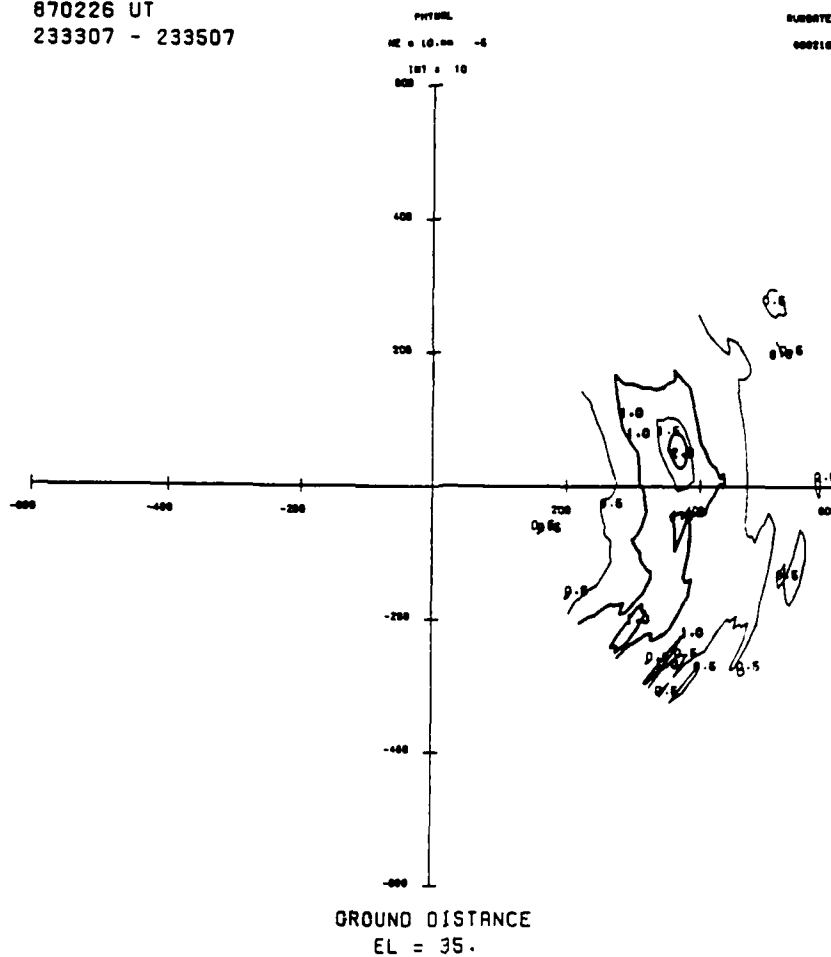GROUND DISTANCE
EL = 35.

400.

200.

0.

-200.

-400.

-400.   -200.   0.   200.   400.

GROUND DISTANCE
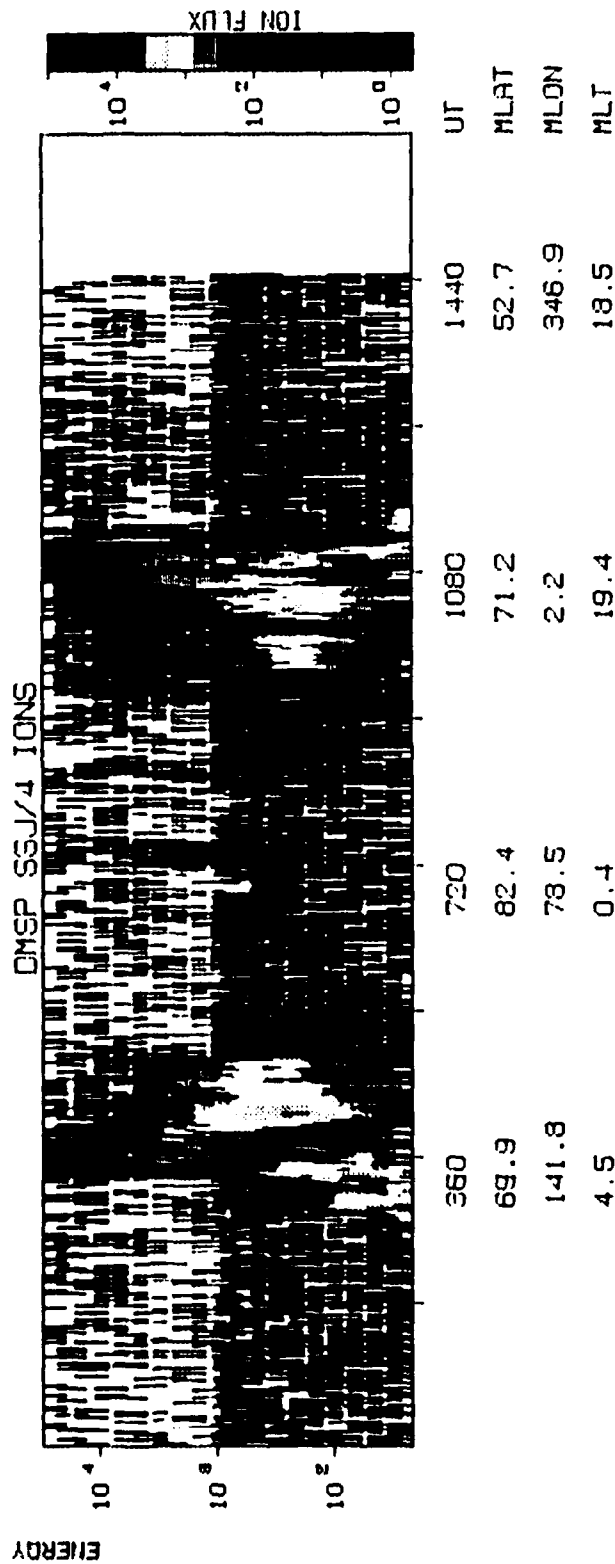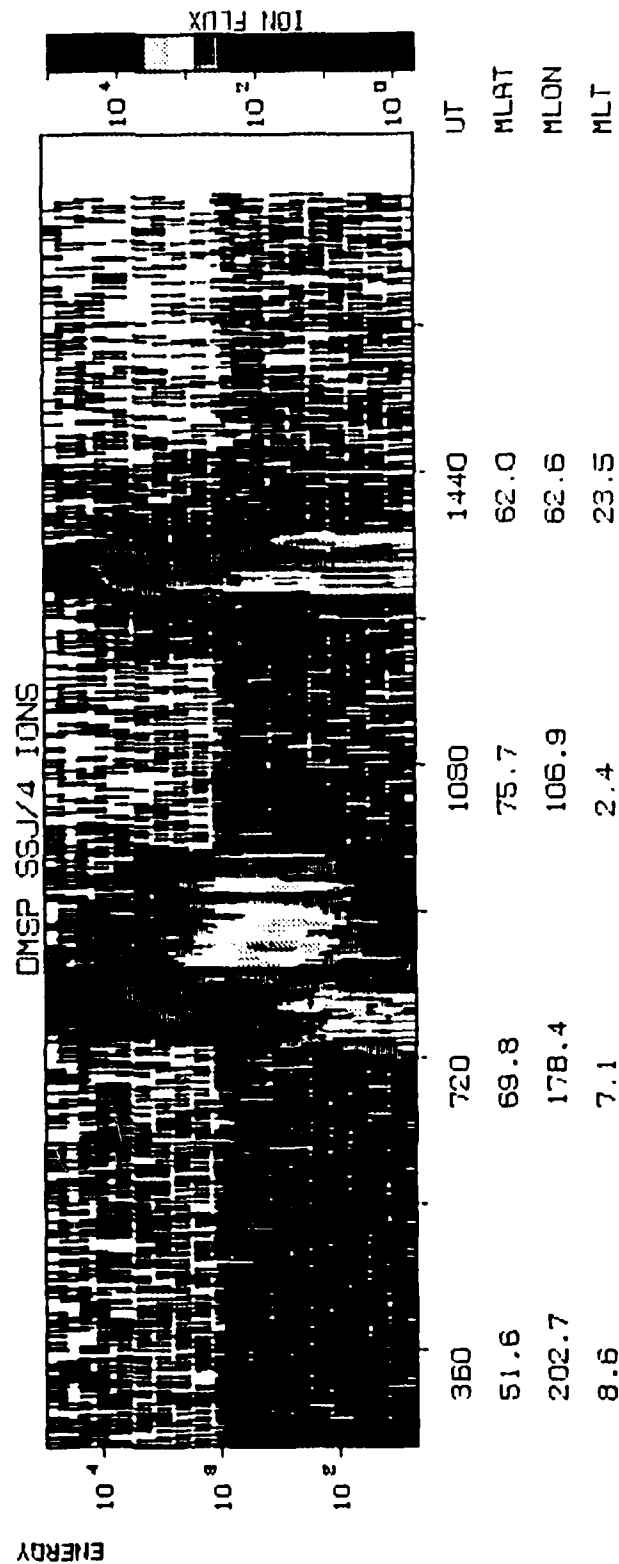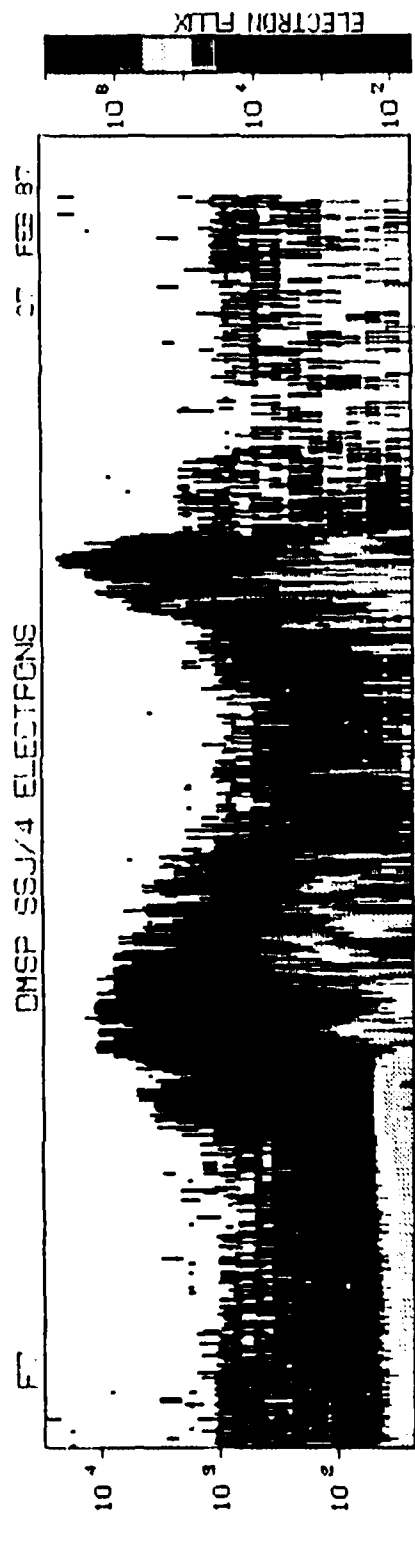
Figure 9(a)

870226 UT
233845 - 234045

GROUND DISTANCE
EL = 35.

400.

200.

0.

-200.

-400.

PRISIS HORIZONTAL VELOCITY   2000 M/S =

-400.   -200.   0.   200.   400.

GROUND DISTANCE
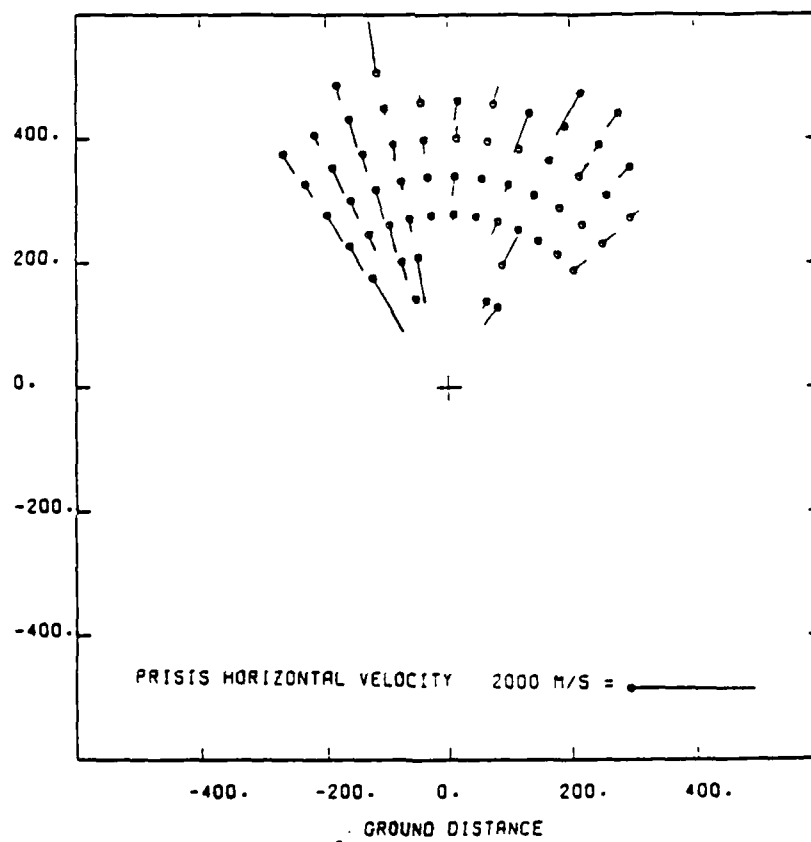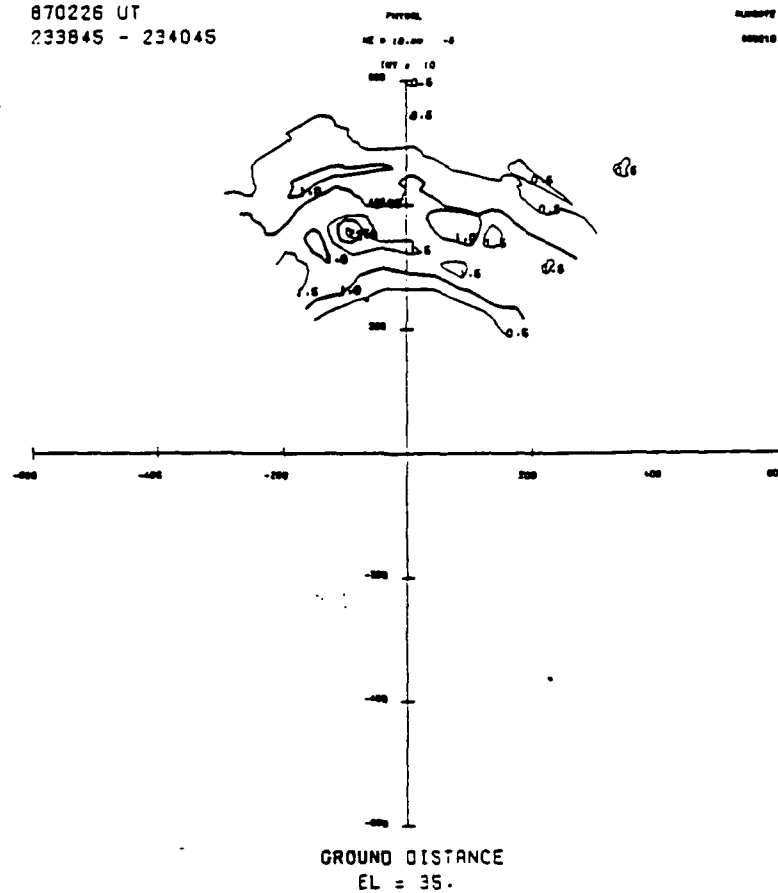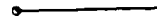
Figure 9 (b)

ELEVATION SCAN
DENPLR: 891220   PULSE = 60
PHYNAL NE=10==-5, 10 SEC INT
870226: 234617 - 234911
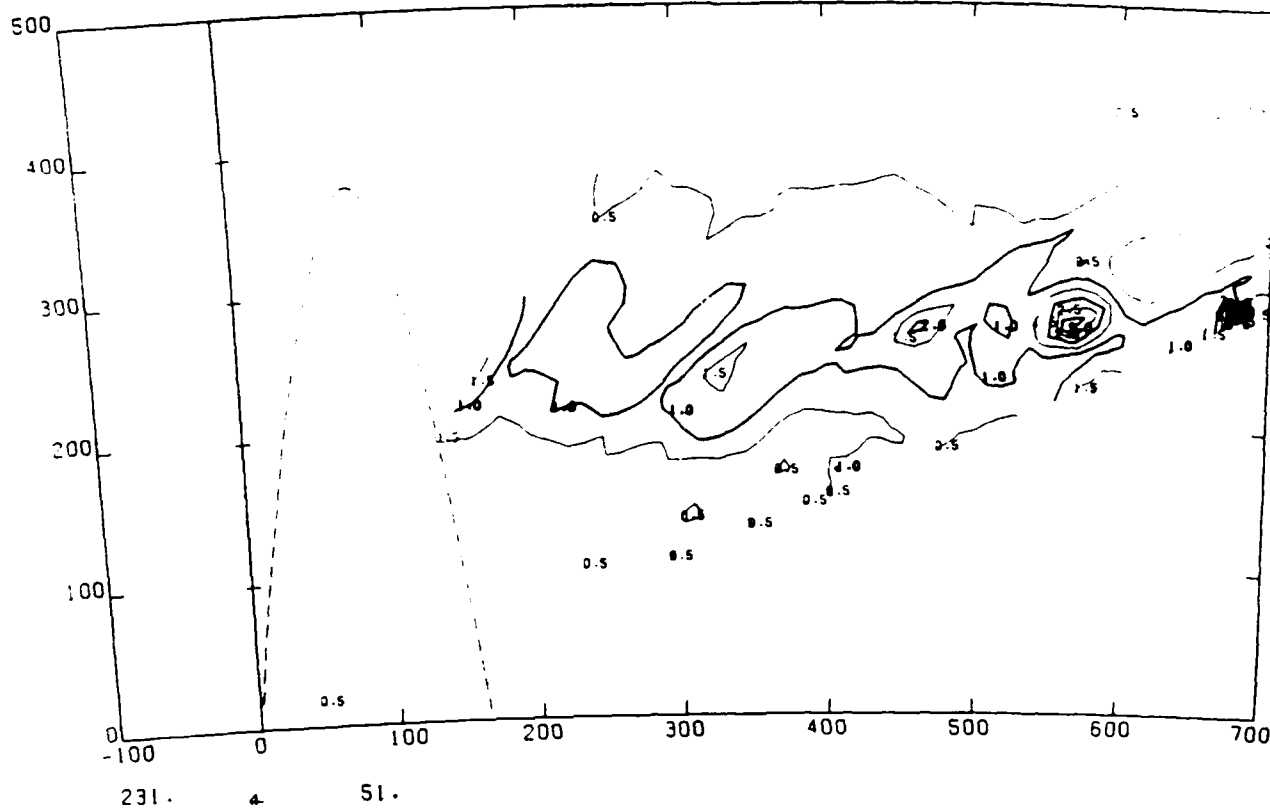
ALLOWED ERROR: 300 (M/S)
2000 M/S = ○————————
LINE OF SIGHT VELOCITY, 10 SEC INT
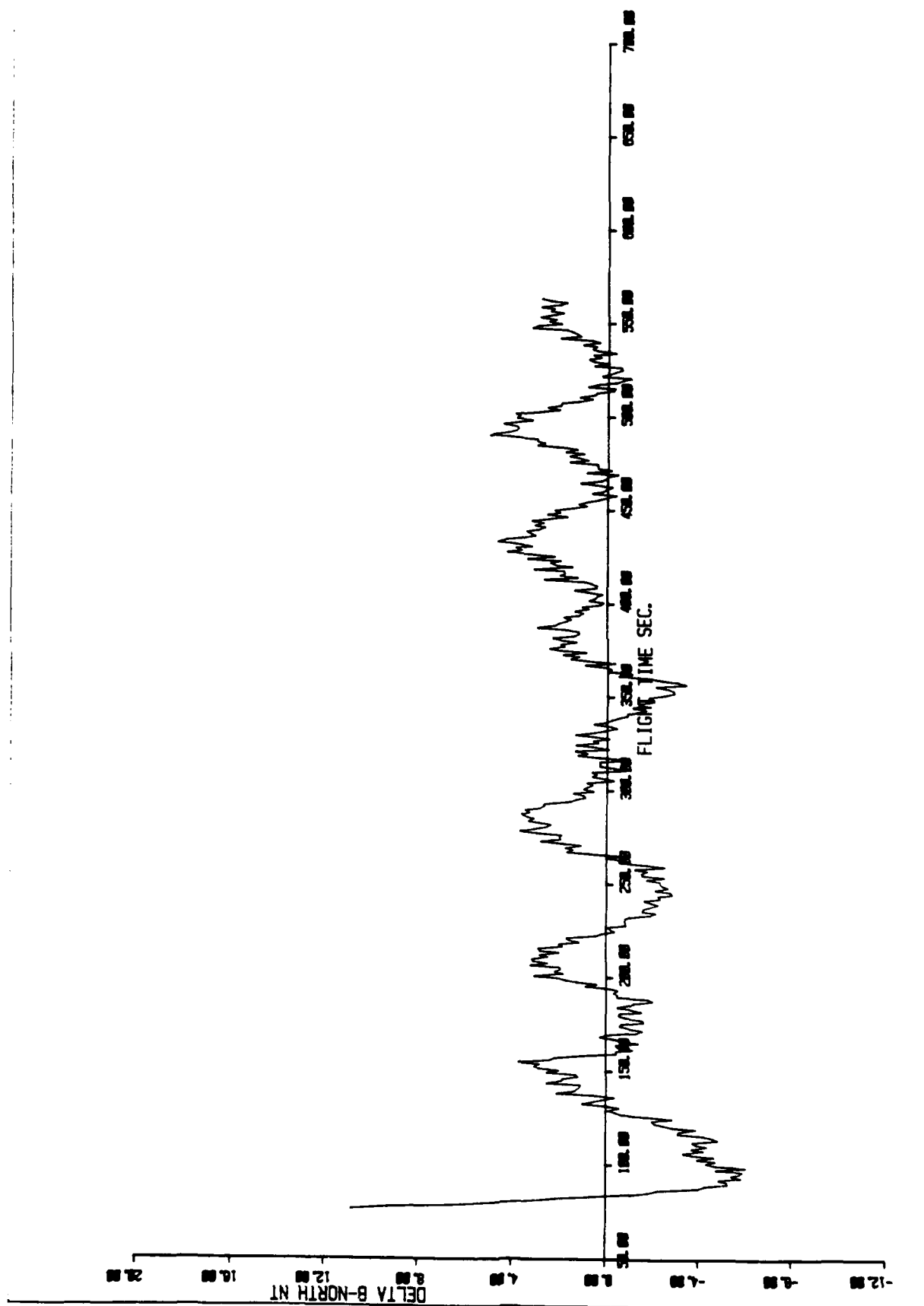870226: 234617 - 234911
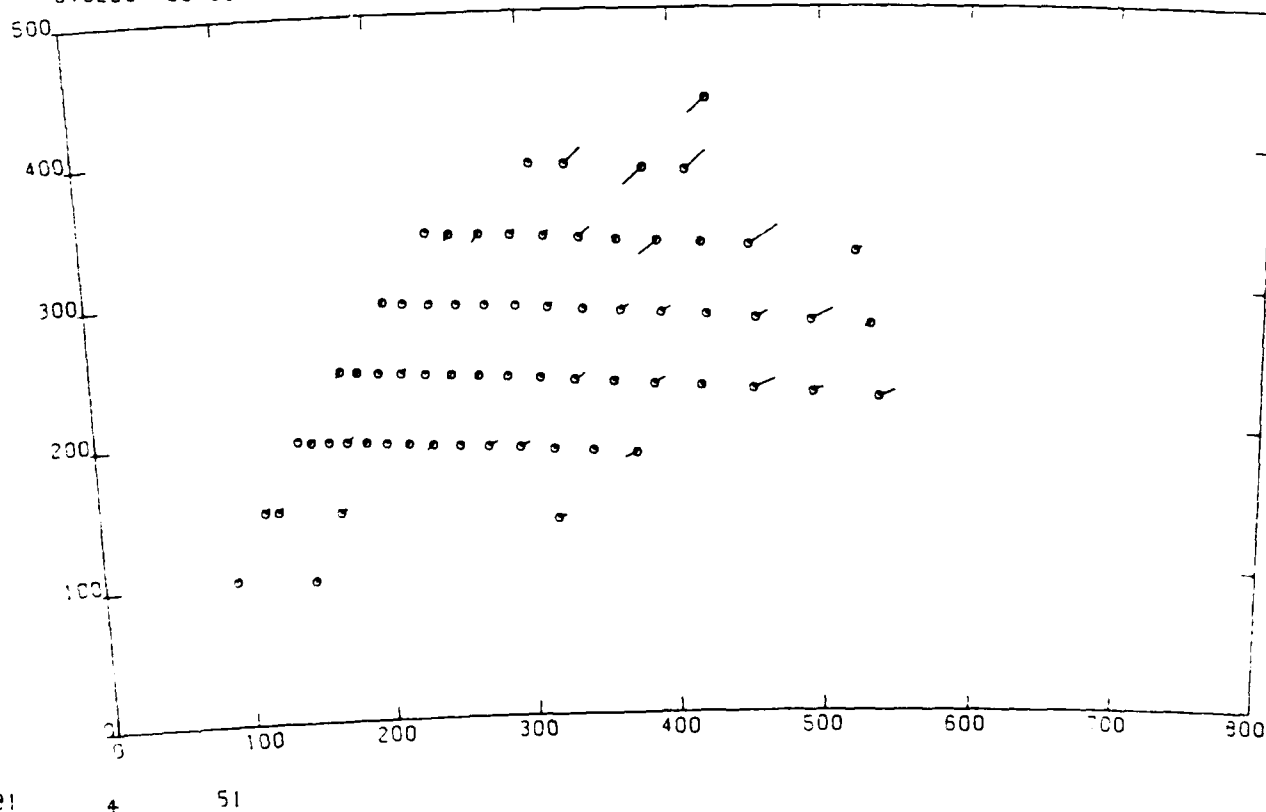
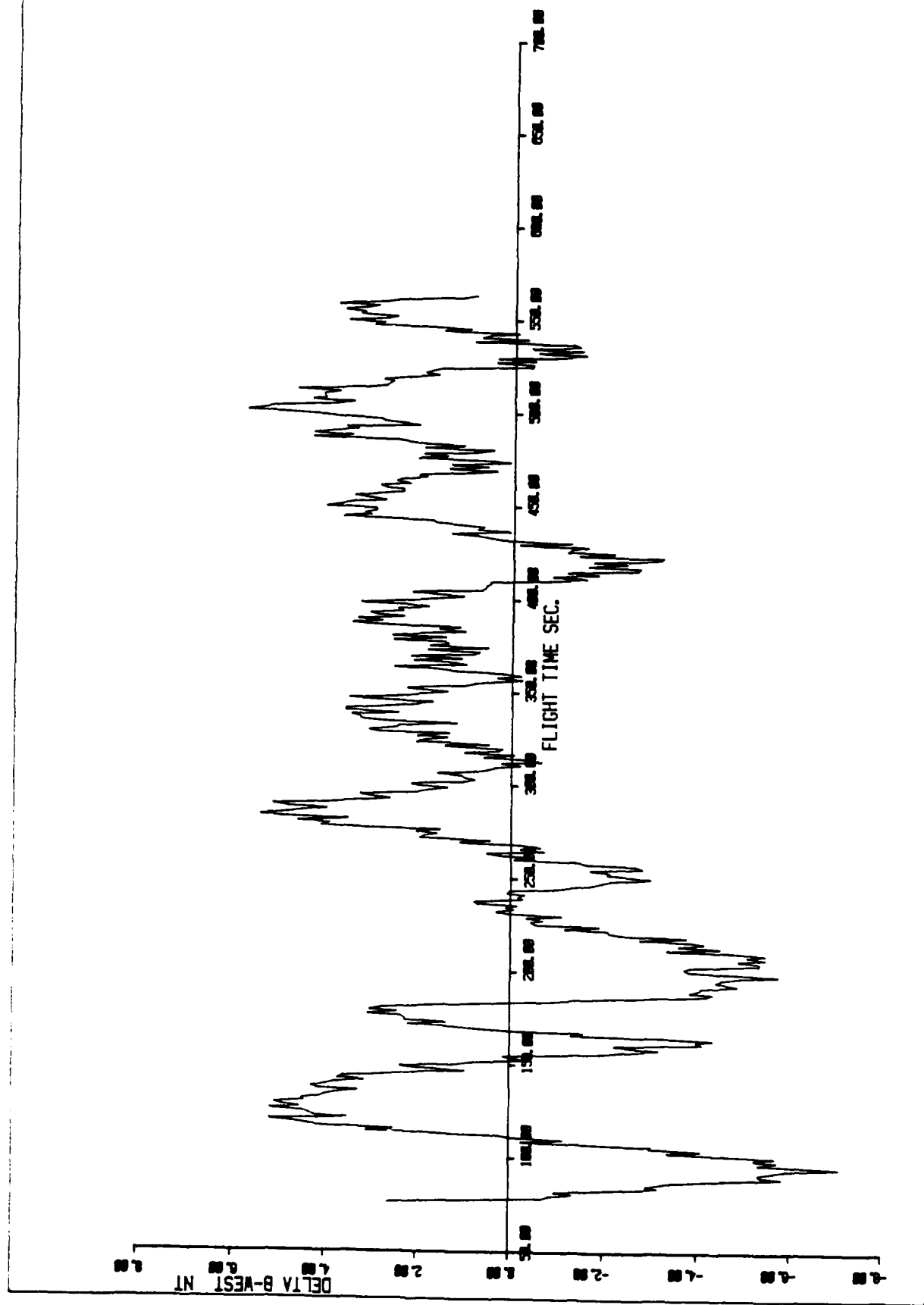**Figure 9 (c)**

POLAR ARCS   Magn Coord
8904046FP   (22°w)

DELTA B-NORTH NT

FLIGHT TIME SEC.

Figure 10 (a)

Figure 10 (b)

Figure 11

February 26, 1987
Drift of barium – jets
NORMAL to the magnetic
meridian plane.

2347 – 2355UT   Vx = 88 m/s, Ey = -4.7 mV/in

I
II
III

ALT (km)

UT

Figure 12

February 26, 1987
Drift of barium – jets
PARALLEL to the magnetic
meridian plane.

2347 – 2350UT   Vy = –134 m/s, Ex = –7.0 mV/m
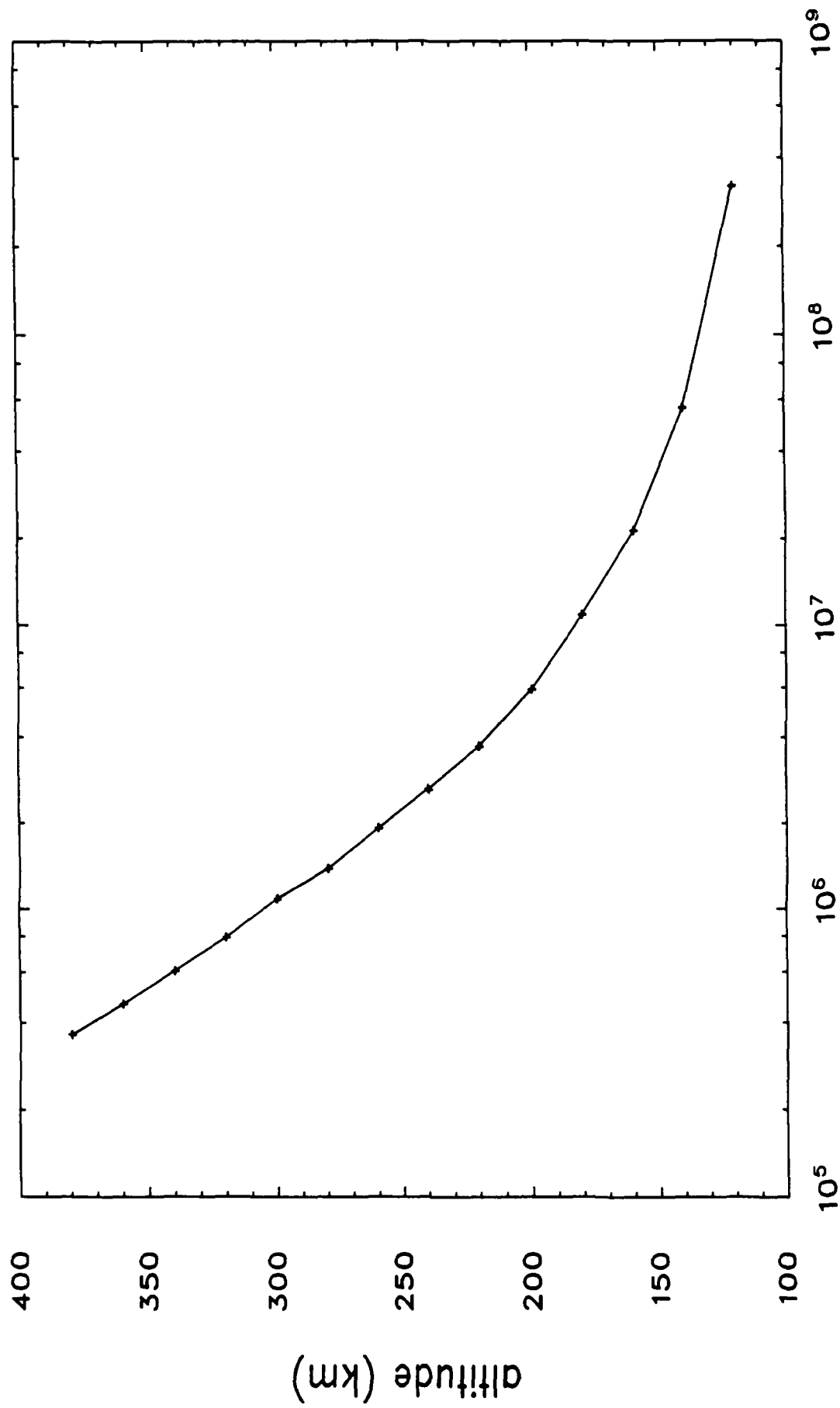2350 – 2355UT   Vy = –420 m/s, Ex = –21.9 mV/m
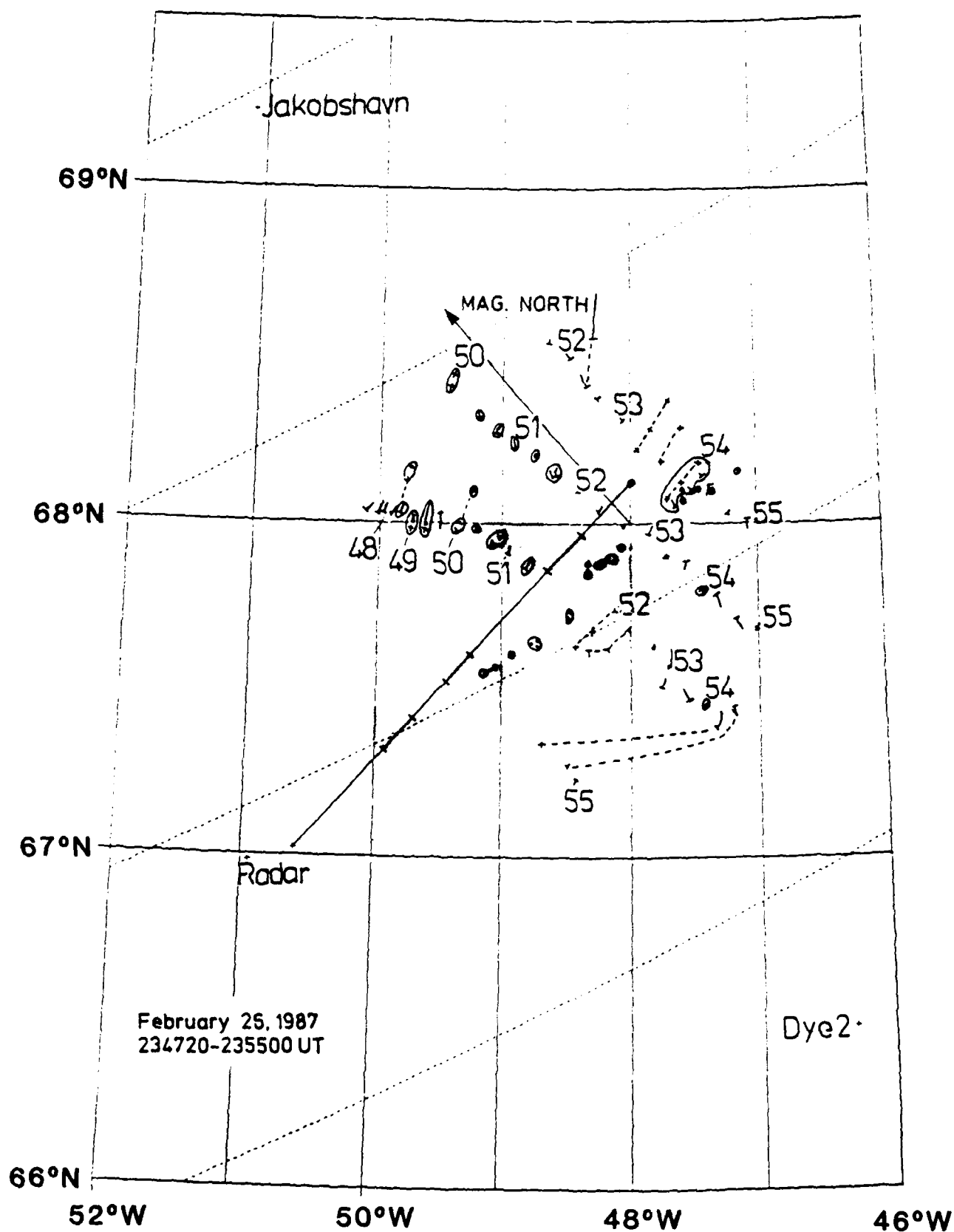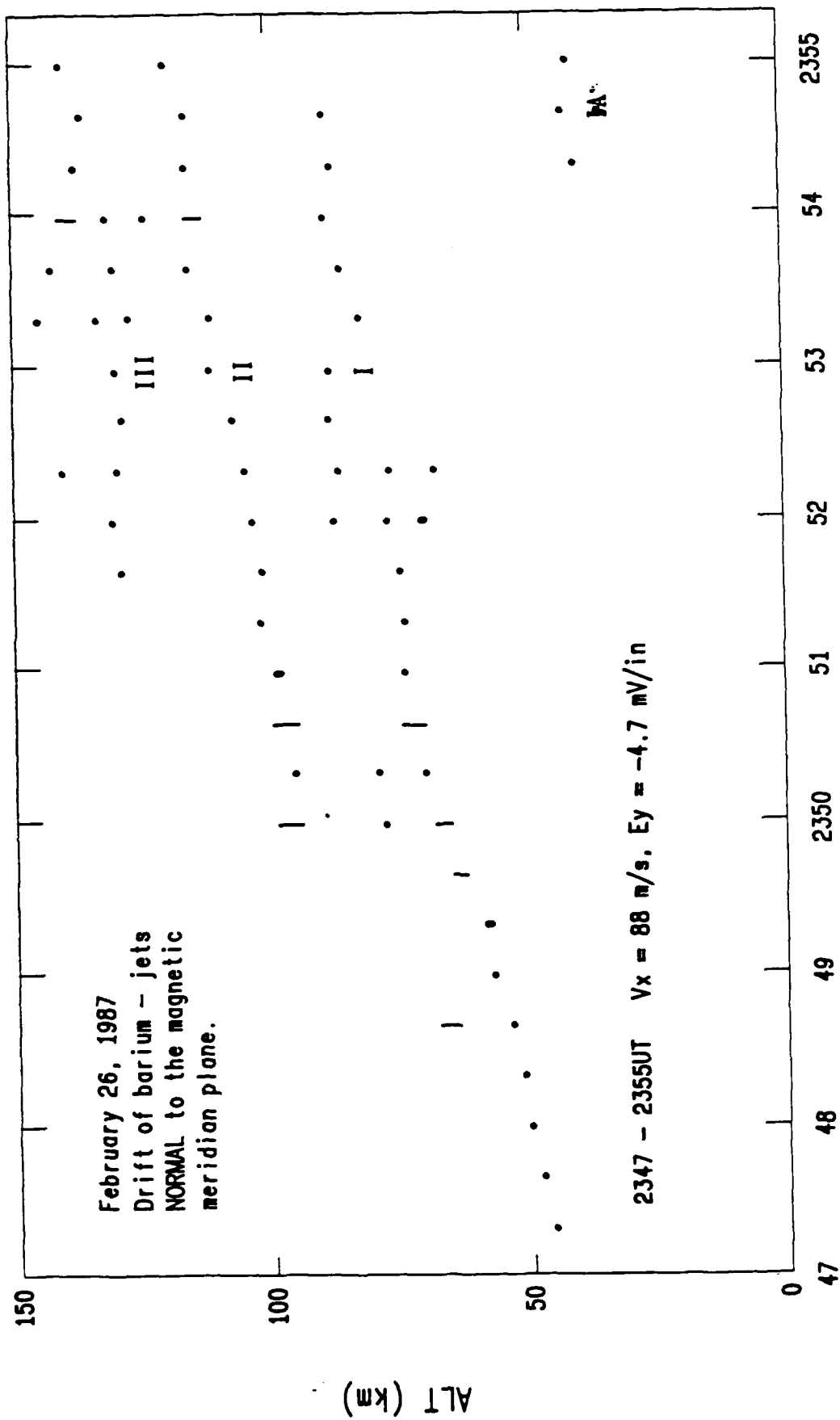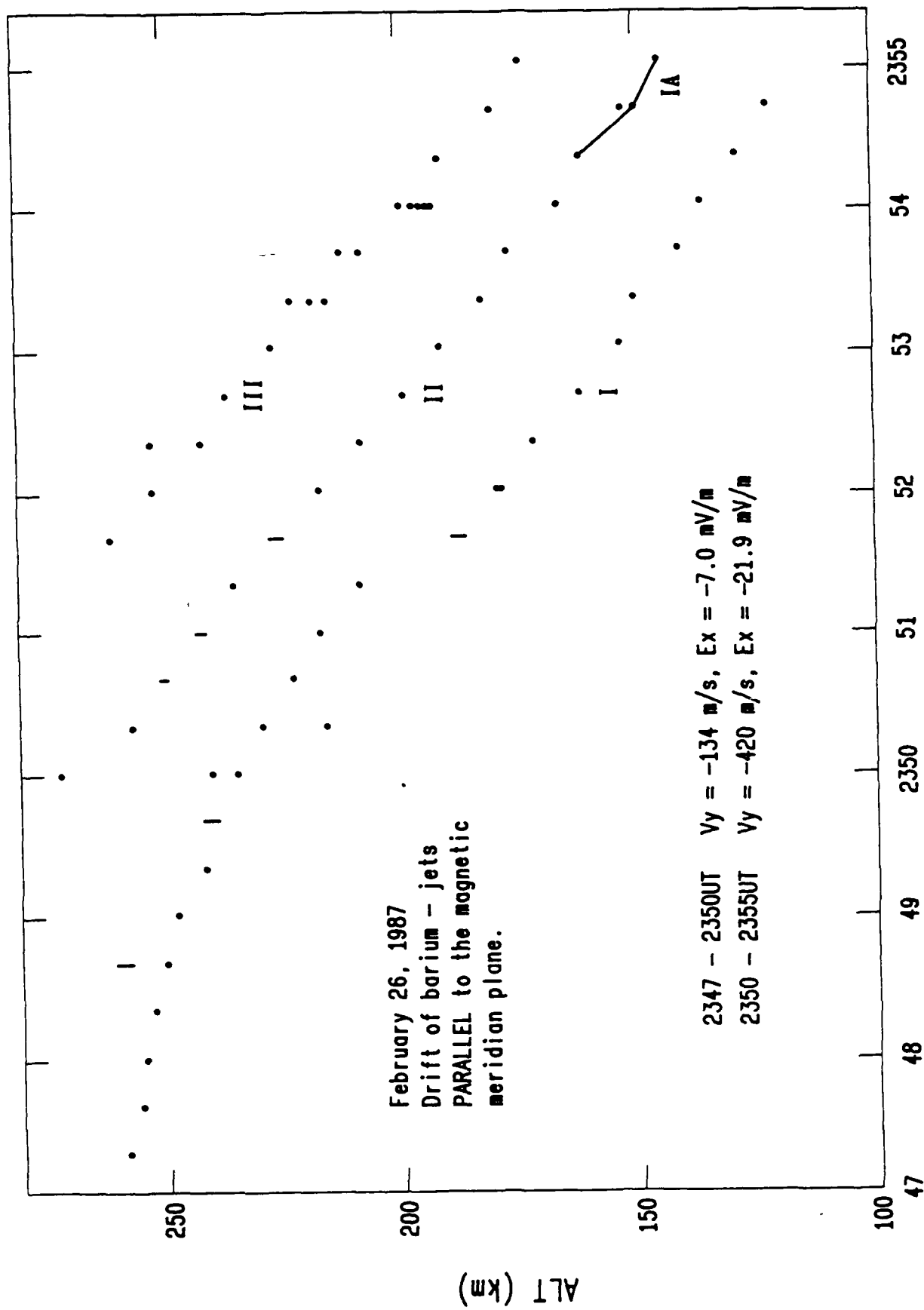
Figure 13

Ion – Neutral Collision Frequency Height Profile

altitude (km)

ion – neutral collision frequency (sec^{-1})

Figure 14

Fri Mar 9, 1990 8:43am